Materials Today Quantum 3 (2024) 100011

Contents lists available at ScienceDirect

Materials Today Quantum

journal homepage: www.sciencedirect.com/journal/materials-today-quantum

Synthesis of strongly confined Bi_2Te_3 quantum dots by pulsed laser ablation in liquids

Rajendra Subedi [a], Francisco Ruiz-Zepeda [b], Qiaohui Zhou [c], Xin Lu [c], Grégory Guisbiers [a,*]

[a] Department of Physics and Astronomy, University of Arkansas at Little Rock, 2801 South University Avenue, Little Rock, AR 72204, USA
[b] Department of Material Chemistry, National Institute of Chemistry, 19 Hajdrihova, Ljubljana 1000, Slovenia
[c] Department of Physics and Engineering Physics, Tulane University, New Orleans, LA 70118, USA

ARTICLE INFO

Keywords:
Quantum dots
Quantum confinement
Bohr radius
Bismuth telluride

ABSTRACT

Quantum dots are semiconductor nanoparticles where electrons' motion is confined within the three physical dimensions of the nanoparticle, such that discretization of energy levels is observed. In this article, quantum dots of Bi_2Te_3, with sizes around 9 ± 2 nm and energy bandgap around ~ 2.8 eV, were successfully synthesized by pulsed laser ablation in liquids. Those dots were found to be within the strong confinement regime.

1. Introduction

Bismuth Telluride (Bi_2Te_3) is an important binary compound made of a post-transition metal, bismuth (Bi), and a chalcogenide element, tellurium (Te) [1]. It occurs naturally on Earth as a mineral called tellurobismuthite [2]. Bi_2Te_3 has a rhombohedral crystalline structure within the $R\bar{3}m$ space group described by the hexagonal unit cell [3,4]. It exhibits a narrow indirect energy bandgap of ~ 0.15 eV and a direct energy bandgap of ~ 0.22 eV at the bulk scale [5,6]. Bi_2Te_3 is a well-known room-temperature thermoelectric material used in thermoelectric coolers, and power generators [7,8]. It is also used in microwave absorbers [9], photodetectors [10], and photovoltaic solar cells [11]. Furthermore, Bi_2Te_3 is also a topological insulator making it suitable for spintronics, and quantum computing devices [12,13].

Nowadays, the scientific community is fascinated by the physico-chemical properties of Bi_2Te_3 at the nanoscale within the quantum confinement regime. However, there are not a lot of papers within the scientific literature reporting the synthesis of Bi_2Te_3 quantum dots (QDs) (Table 1). In this work, we successfully synthesized Bi_2Te_3 QDs for the very first time by Pulsed laser ablation in liquids (PLAL) technique using a bottom-ablation synthesis protocol. This type of bottom-ablation synthesis protocol is advantageous for producing smaller nanoparticles compared to a top-ablation protocol [14,15]. PLAL is a cost-effective and eco-friendly technique generating highly pure QDs or nanoparticles. Moreover, various shapes and sizes can be achieved by changing the laser parameters and solvents. The process of forming QDs through PLAL involves absorbing the laser beam by the target and the solvent; consequently, producing a plasma. This plasma leads to the creation of a cavitation bubble within the liquid. The ions and electrons present in the cavitation bubble react together to form the QDs [16,17].

2. Materials and methods

2.1. PLAL synthesis

A Q-switched Nd:YAG laser from Electro Scientific Industries was used to synthesize Bi_2Te_3 QDs. The laser beam was emitted in the infrared region at 1064 nm. Bismuth-telluride flakes (@99.99 % from Sigma-Aldrich) were used as a target. Before irradiation, the target was cleaned by an ultrasonic cleaner using acetone for 15 minutes. The target was put inside a 50 ml single-neck glass flask and was immersed in 10 ml of acetone. The infrared laser beam was reflected onto a flat mirror, inclined at 45° with respect to the laser rail. The laser beam was focused on the target's surface by using a bi-convex lens having a focal length of 16 mm which was placed between the mirror and the target. The power of the laser was measured around 12.5 W with an energy per pulse of 12.5 mJ/pulse as the repetition rate was fixed at 1 kHz. The average spot size of the laser beam onto the target was measured to be around $\sim 110 \pm 28$ μm. The laser fluence was consequently calculated to be $\sim 131 \pm 33$ J cm^{-2}. The target was finally irradiated for 5 minutes.

* Corresponding author.
E-mail address: gxguisbiers@ualr.edu (G. Guisbiers).

https://doi.org/10.1016/j.mtquan.2024.100011
Received 17 June 2024; Received in revised form 8 August 2024; Accepted 21 August 2024
Available online 22 August 2024

Table 1
List of peer-reviewed papers reporting the synthesis of bismuth telluride quantum dots using various techniques.

Synthesis technique	Size	Shape	Energy bandgap	Environment	Ref.
Hydrothermal	43 ± 3 nm and 20 ± 3 nm	Spherical	Unknown	Colloid	[9]
Wet-chemical	35 nm	Spherical	1.20 eV	Colloid	[18]
Wet-chemical	17.5 ± 1.8 nm	Rhombohedral	Unknown	Colloid	[19]
Thermo-chemical	4–14 nm	Spherical	3.12–2.69 eV	Within a glass matrix	[20]
Thermo-chemical	6 by 10 nm	Rod	2.49 eV	Within a glass matrix	[20]
Solvothermal	< 10 nm	Spherical	Unknown	Colloid	[21]
PLAL	9 ± 2 nm	Spherical	2.8 eV	Colloid	This work

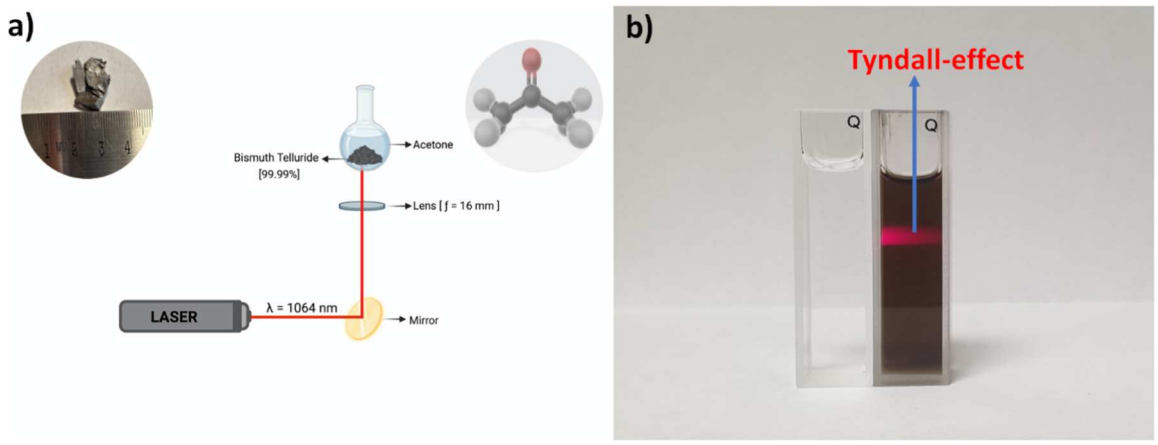

Fig. 1. a) Sketch of the PLAL synthesis protocol showing the "Bottom-ablation" setup used to synthesize Bi_2Te_3 QDs. Inset: Bulk Bi_2Te_3Target used for irradiation (left), and structure of acetone molecule (right). **b)** Photo: The left cuvette contains a standard solution of acetone and the right one contains a colloid synthesized by PLAL. The "*Tyndall effect*" is only observed in the right cuvette.

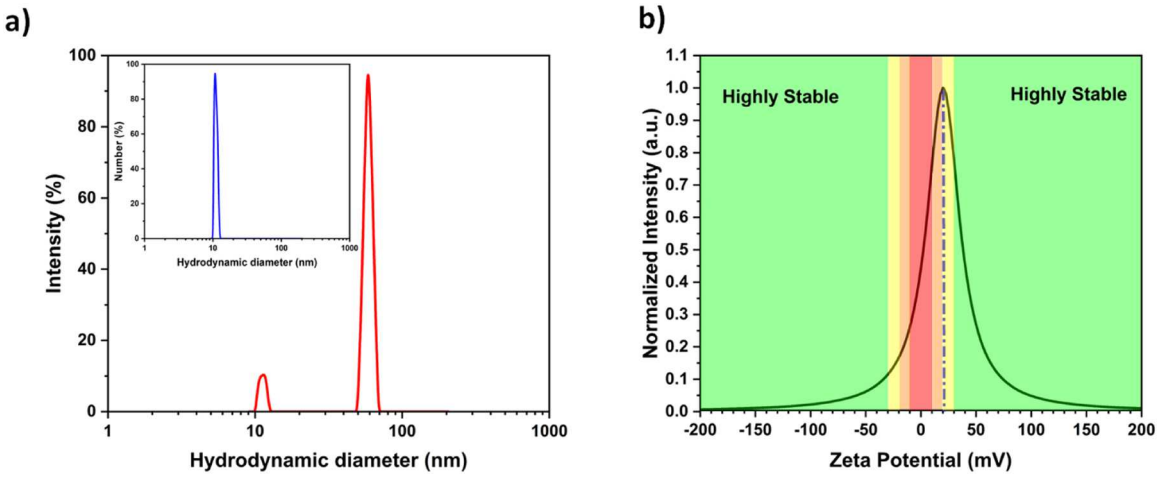

Fig. 2. Size distribution and stability **a)** Size distribution (Intensity versus size) measured by DLS. Inset: Number of particles versus size **c)** Zeta potential of colloid containing Bi_2Te_3 QDs. The colloidal stability is color-coded: highly unstable (red), relatively stable (orange), moderately stable (yellow) and highly stable (green).

2.2. Physico-chemical characterization

Immediately after synthesis, the colloid containing the Bi_2Te_3 QDs was stored in a 10 ml opaque microtube for preservation. The QDs were then characterized by Dynamic Light Scattering (DLS -NanoBrook 90Plus from Brookhaven Instruments Corporation), UV–visible spectroscopy (Cary 60 from Agilent), Raman Spectroscopy (Home-made system), X-ray diffraction (XRD-Miniflex 600 from Rigaku) and Transmission Electron Microscopy and Scanning Transmission Electron Microscopy (TEM and STEM, respectively). Raman scattering measurements were carried out by using a home-built setup. The measurements were conducted in a backscattering configuration excited with a solid-state green laser ($\lambda = 532$ nm). To reach the ultra-low frequency Raman shift of ~ 10 cm^{-1}, we used the volume Bragg grating filters (OptiGrate) to block the laser line. The backscattered signal was collected through a 100 × objective and dispersed by an 1800 g/mm grating before the liquid nitrogen-cooled charge coupled device (Princeton Instruments, PyLoN 1340 × 400 pixels CCD). TEM and STEM were carried out on a JEOL ARM 200 CF microscope operated at 80 kV. Chemical mappings were performed using a SDD JEOL Centurio Energy-Dispersive X-ray (EDX) spectrometer. For the DLS and UV–visible spectroscopy, 3 ml of colloidal solution were placed in a quartz cuvette for characterization. For TEM/STEM characterization, a droplet of colloidal solution was dropped on a TEM copper grid, exposing it

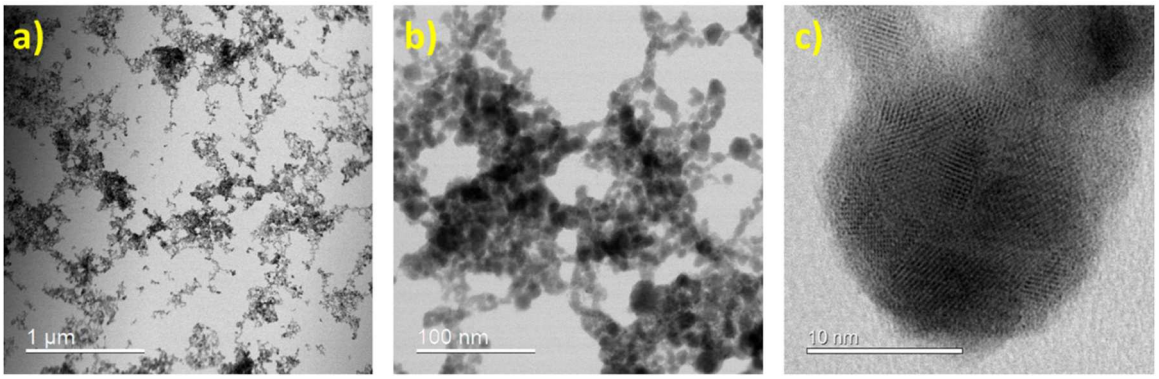

Fig. 3. a)–c) STEM-BF images of the Bi_2Te_3 QDs at different magnifications.

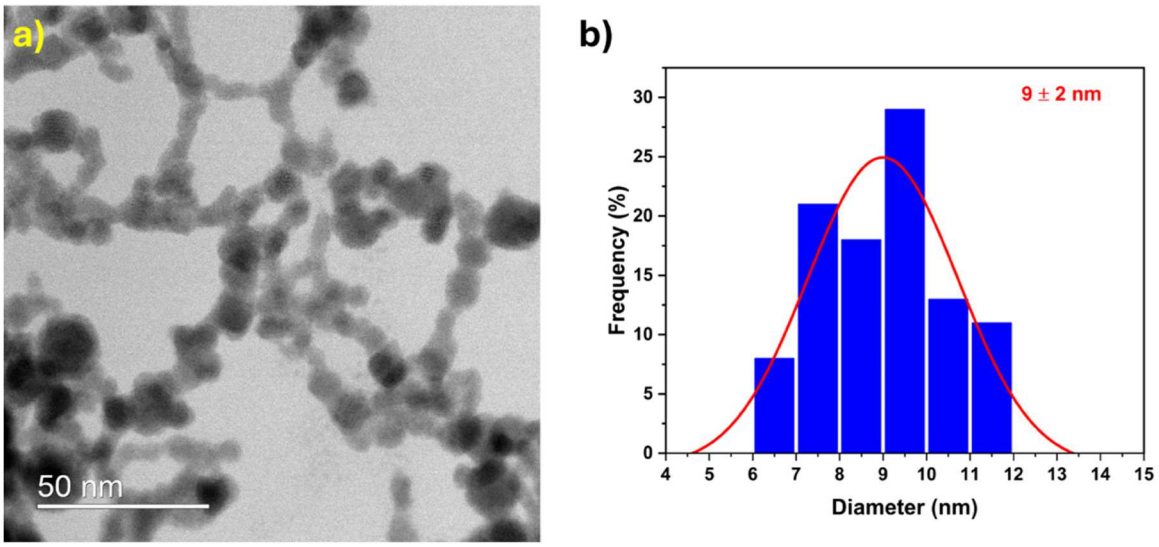

Fig. 4. a) STEM-BF image of the Bi_2Te_3 QDs. **b)** Histogram representing the particle size distribution of the STEM image shown in a).

minimum to air, and let it continue to dry completely in a vacuum environment (10^{-3} Pa). For the Raman spectroscopy and X-ray diffraction, the colloid was centrifuged at 13,000 rpm for 60 min using the Sorvall Legend micro 17 from Thermo Scientific, to collect enough QDs and remove the excess of solvent. The sedimented QDs were then recovered and dried into a glovebox before their Raman and XRD characterization.

3. Results and discussion

The PLAL setup to create Bi_2Te_3 QDs is shown in Fig. 1a. This type of setup is known as the "*Bottom-ablation*" technique because the laser hits the target from underneath the container. The target used for the synthesis is a pure Bi_2Te_3 target (inset Fig. 1a). The sample containing the Bi_2Te_3 QDs is shown on Fig. 1b. For comparison purpose, a cuvette containing only the solvent (acetone in this case) is also shown on Fig. 1b. When the laser pointer's beam is shined through the colloid, the light is scattered due to the presence of the QDs. This effect is known as the *"Tyndall effect"* [22].

After synthesis, the size distribution of the particles and their stability was determined by DLS. Two different intensity peaks centered around ~ 56 ± 7 nm and ~ 12 ± 2 nm appeared on the spectra (Fig. 2a) displaying two different-sized populations. However, the diameter measured by the DLS is not the physical diameter of the nanoparticles but the hydrodynamic diameter [23]. Consequently, it may be misleading to the reader that there is a huge population of particles having a size around ~ 56 nm. Indeed, it is important to understand that the scattering of light is proportional to the 6th power of the radius of the particle [23]. Therefore, larger particles will scatter more light than smaller ones; so, the intensity of each peak should not be used to compare the number of nanoparticles within each population. To do that, the number of nanoparticles versus size needs to be used (Inset Fig. 2a). From the inset, the second peak centered at around ~ 56 nm disappeared and only survives the first one, indicating that most nanoparticles had a size around ~ 12 nm. The presence of the peak around ~ 56 nm may be due to the flocculation of the particles. Indeed, the zeta potential of the Bi_2Te_3 QDs was found to be around ~ 20 ± 12 mV at a pH of 5.8 ± 0.3 (Fig. 2b). The magnitude of zeta potential indicates the degree of electrostatic repulsion or attraction between the particles in suspension, which is an important parameter for understanding the stability of the particles in the colloid. Colloids with zeta potential values of ± 0–10 mV, ± 10–20 mV and ± 20–30 mV and > ± 30 mV qualify as highly unstable, relatively stable, moderately stable and highly stable, respectively [23]. The Bi_2Te_3 QDs synthesized by PLAL qualify as relatively stable but could flocculate over time.

The size of the Bi_2Te_3 QDs has also been determined from images obtained by STEM (Fig. 3). Fig. 3a–c show STEM Bright Field (BF) images of the Bi_2Te_3 QDs under different magnifications. The shape of QDs is quasi-spherical (Fig. 4a), and most of the sizes ranges from 6 nm to 12 nm, with an average value at 9 ± 2 nm, as can be seen from the histogram shown in Fig. 4b. The sizes of the QDs measured by STEM are in excellent agreement with the size determined by DLS. As the size of

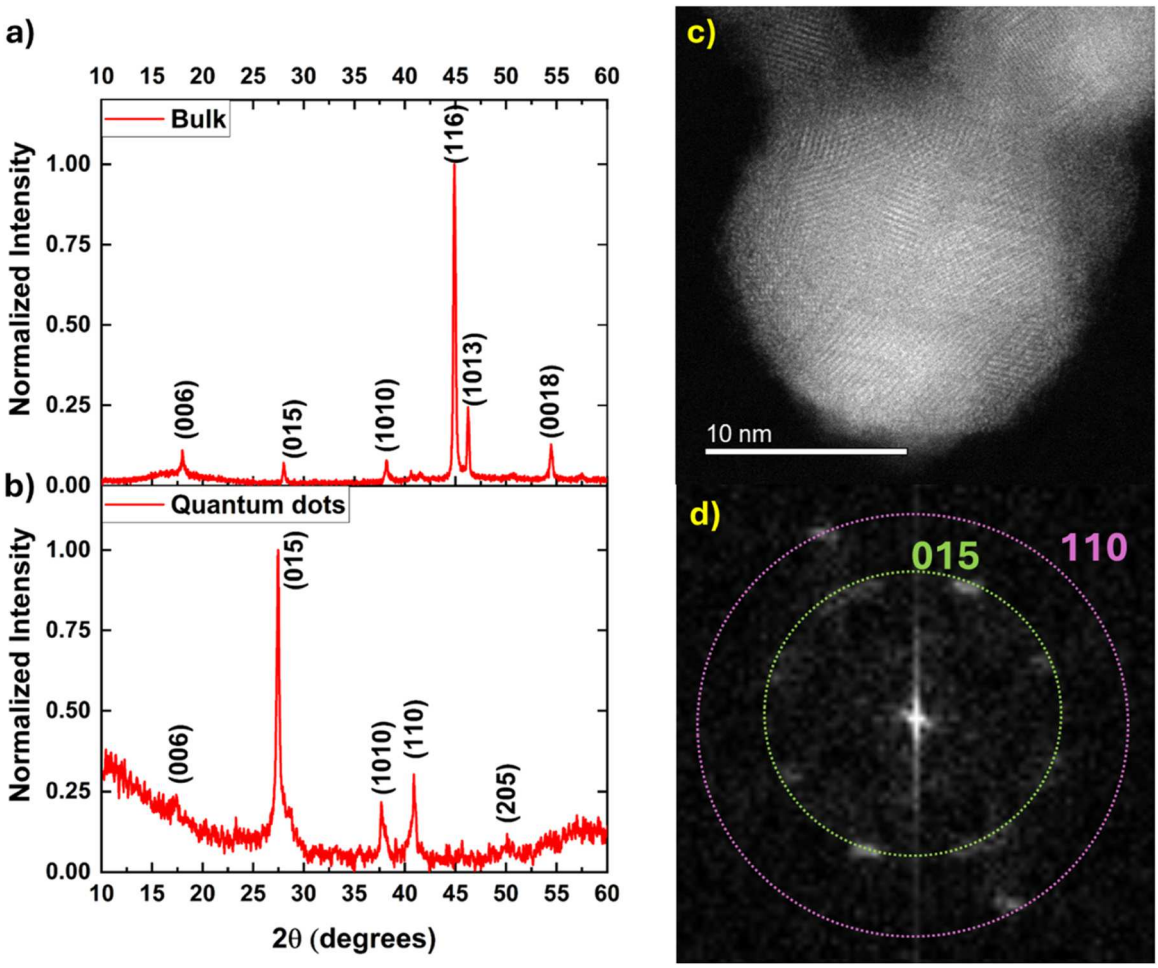

Fig. 5. **a)** XRD pattern of the Bi_2Te_3 bulk target. **b)** XRD pattern of Bi_2Te_3 QDs. The XRD Peak positions were identified based on the crystallographic open database 9011962. **c)** STEM-Annular Dark Field (ADF) image of one single Bi_2Te_3 QD. **d)** FFT of the image shown in c). The plane indexing corresponds to the Bi_2Te_3 rhombohedral structure.

the nanoparticles is less than Bi_2Te_3 electron's Bohr's radius i.e. 57 nm [20,24] and hole's Bohr's radius i.e. 45 nm [24]; then it can be concluded that the nanoparticles synthesized in this manuscript are in the strong confinement regime [25].

The chemical composition and crystalline structure of the bulk target and QDs were analyzed by XRD (Fig. 5a, b). All the XRD peaks located at 17.5° (006), 27.6° (015), 37.8° (1010), 41.0° (110), 44.9° (116), 45.9° (1013), 50.3° (205) and 54.2 (0018) were matching the rhombohedral lattice structure of Bi_2Te_3. By comparing both diffraction patterns, it can be noticed that the growth direction of QDs (015) did not follow the growth orientation of the target (116); therefore, the QDs were not created by laser fragmentation but by laser ablation involving melting and recrystallization. By using the Scherrer equation, the crystallite size was determined to be around 3.5±0.1 nm meaning that the Bi_2Te_3 QDs were polycrystalline as shown on Fig. 5c. Moreover, the Fast-Fourier-Transform (FFT) performed on Fig. 5c confirmed the rhombohedral structure of the QD (Fig. 5d).

Raman spectroscopy was performed on the bulk Bi_2Te_3 target as well as on the Bi_2Te_3 QDs synthesized by PLAL to study their chemical composition and quantum confinement as shown in Fig. 6. By comparing the two Raman spectra, it can be seen that the non-active Raman modes A^1_{1u} and A^2_{1u} became active at the quantum scale while the active Raman modes A^1_{1g}, E^2_g and A^2_{1g} were blue-shifted, confirming the quantum confinement. The A_{1g} mode ("*out-of-plane vibrations*") represents the vibration of atoms along the c-axis, i.e., the plane perpendicular to the basal plane; whereas the E_g mode ("*in-plane vibrations*") represents the vibrations within the basal plane. In the A^1_{1g} mode, the bismuth and tellurium atoms vibrate in phase while in the A^2_{1g} and E^2_g modes, they vibrate in opposite phase. The A_{1u} modes become active because the confinement breaks down the symmetry along the c-axis. Another interesting observation is that the intensity of the out-of plane vibrations (A_{1g}) is higher for the Bi_2Te_3 quantum dots than for the Bi_2Te_3 bulk; while the in-plane vibrations (E_g) are higher in intensity for the Bi_2Te_3 bulk than for the Bi_2Te_3 quantum dots. The decreased intensity of the in-plane vibrational modes and the increased intensity of some out-of-plane vibrational modes seems to be another indication of the quantum confinement. Indeed, the E^2_g vibrational mode lost ~ 75 % of its intensity while the A^2_{1g} vibrational mode gained ~ 50 % when comparing the bulk with the quantum dot. A similar behavior has already been noticed in a few quintuple layers of Bi_2Te_3 by Shahil et al. [26]. Finally, the Raman peak positions were consistent with the literature [27–29].

To confirm the chemical composition of the QDs, EDXS elemental chemical mapping was performed on the QDs (Fig. 7). Bi and Te can be seen uniformly distributed all over the particle.

The optical investigation was done using UV–vis spectroscopy as shown in the Fig. 8a. The energy band gap was determined by using the Tauc plot methodology [30,31] revealing a value around ~ 2.8 eV (Fig. 8b). This value is in very good agreement with Panmand et al. [20], who found a direct energy bandgap between 3.12 eV and 2.69 eV for Bi_2Te_3 nanoparticles having sizes between 4 nm and 14 nm, respectively (Table 1). Theoretically, as particle size decreases there is an increase of

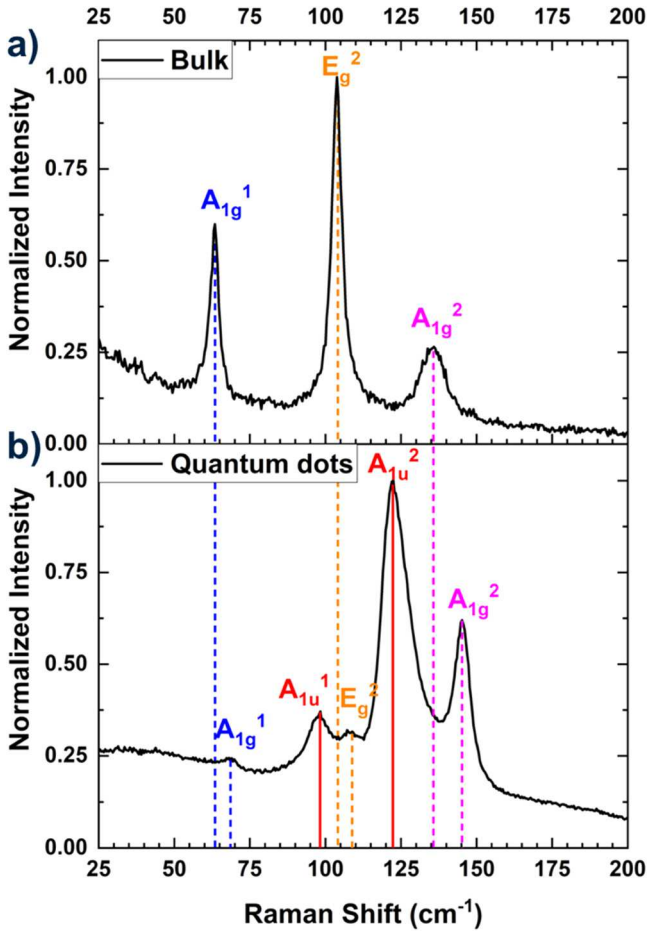

Fig. 6. a) Raman spectra of Bulk Bi_2Te_3 target for reference purposes. **b)** Raman spectra of Bi_2Te_3 QDs confirming the quantum confinement.

the energy bandgap due to surface effects and quantum effects [25]. Here, both effects contribute to the increased value of the energy bandgap. Firstly, by decreasing the size of the Bi_2Te_3 target by PLAL, the surface to volume ratio of the synthesized nanoparticles increased (surface effects) and consequently their energy bandgap too. Secondly, as the diameter of the Bi_2Te_3 nanoparticles synthesized by PLAL are below both the electron Bohr radius (~ 57 nm) [20,24] and hole Bohr radius (~ 45 nm) [24] of Bi_2Te_3, they are within the strong confinement regime (quantum effects) [25]. Generally, the size effect on the energy bandgap of nanoparticles can be predicted by using a scaling law where the energy bandgap is determined by a linear relationship of the reciprocal size of the nanoparticle [32]. However, in this case, two experimental data points deviate from the linear relationship below a given reciprocal size (~ 0.07 nm^{-1}); consequently, indicating a pure quantum behavior (Fig. 8c).

4. Conclusions

In conclusions, Bi_2Te_3 QDs have been successfully synthesized for the very first time by PLAL. The size of the QDs was measured to be around 9 ± 2 nm which is much smaller than the electron and hole Bohr radius of Bi_2Te_3, signifying a strong quantum confinement. Consequently, the energy bandgap of QDs (~ 2.8 eV) displayed a much larger value than the bulk energy bandgap of Bi_2Te_3 (~ 0.15 eV). Quantum confinement was further confirmed by Raman spectroscopy where Raman peaks were blue-shifted and infrared peaks popped up in the Raman spectra. More work is now in progress to include those Bi_2Te_3 QDs into optoelectronic devices.

CRediT authorship contribution statement

Rajendra Subedi: Writing – original draft, Visualization, Investigation, Formal analysis. **Francisco Ruiz-Zepeda:** Writing – review & editing, Visualization, Validation, Resources, Investigation, Formal analysis. **Qiaohui Zhou:** Investigation, Formal analysis. **Xin Lu:** Writing – review & editing, Supervision, Resources. **Gregory Guisbiers:** Writing – review & editing, Visualization, Validation, Supervision, Resources, Project administration, Funding acquisition, Conceptualization.

Funding Declaration

This work was supported by the National Science Foundation under Grant no. 2228891.

Declaration of Competing Interest

The authors declare that they have no known competing financial interests or personal relationships that could have appeared to influence the work reported in this paper.

Declaration of Competing Interest

The authors declare the following financial interests/personal relationships which may be considered as potential competing interests: Gregory Guisbiers reports financial support was provided by National Science Foundation. Rajendra Subedi reports financial support was provided by National Science Foundation. If there are other authors, they declare that they have no known competing financial interests or personal relationships that could have appeared to influence the work reported in this paper.

Data availability

Data will be made available on request.

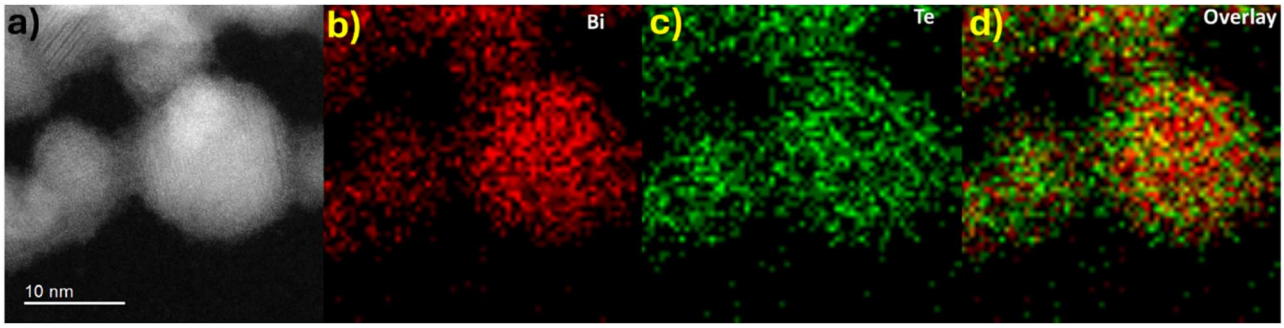

Fig. 7. EDXS elemental chemical mapping of Bi_2Te_3 QDs. Bi and Te are indicated in red and green, respectively.

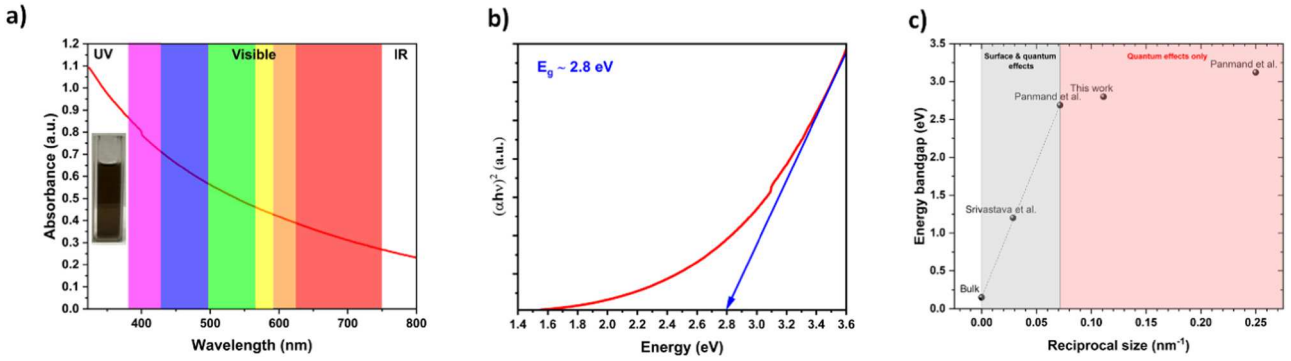

Fig. 8. Optical investigation. **a)** UV–visible spectra of the colloid. Inset: Colloid used for the UV–vis spectroscopy. **b)** Tauc-plot displaying the energy bandgap of ~ 2.8 eV of Bi_2Te_3 QDs. **c)** Graph comparing the energy bandgap of the Bi_2Te_3 quantum dots from this work with others from the literature (Table 1).

Acknowledgements

F.R.-Z. acknowledges the European Research Council (ERC) Starting Grant 123STABLE (Grant agreement ID: 852208).

References

[1] Y. Wang, Y. Zhao, X. Ding, L. Qiao, Recent advances in the electrochemistry of layered post-transition metal chalcogenide nanomaterials for hydrogen evolution reaction, J. Energy Chem. 60 (2021) 451–479.
[2] R.M. Thompson, The telluride minerals and their occurrence in Canada, Am. Mineral.: J. Earth Planet. Mater. 34 (1949) 341–382.
[3] M.S. Shalaby, N.M. Yousif, L.A. Wahab, H.M. Hashem, Structural, optical, and physical properties investigations of Bi_2Te_3 topological insulator nanocomposites exposure to ^{60}Co γ-rays, Mater. Sci. Eng. B-Adv. 271 (2021) 115246.
[4] Y. Hosokawa, K. Tomita, M. Takashiri, Growth of single-crystalline Bi_2Te_3 hexagonal nanoplates with and without single nanopores during temperature-controlled solvothermal synthesis, Sci. Rep. 9 (2019) 10790.
[5] P. Larson, S.D. Mahanti, M.G. Kanatzidis, Electronic structure and transport of Bi_2Te_3 and $BaBiTe_3$, Phys. Rev. B 61 (12) (2000) 8162–8171.
[6] G.A. Thomas, D.H. Rapkine, R.B. Vandover, L.F. Mattheiss, W.A. Sunder, L. F. Schneemeyer, J.V. Waszczak, Large electronic-density increase on cooling a layered metal-doped Bi2te3, Phys. Rev. B 46 (3) (1992) 1553–1556.
[7] I.T. Witting, T.C. Chasapis, F. Ricci, M. Peters, N.A. Heinz, G. Hautier, G.J. Snyder, The thermoelectric properties of bismuth telluride, Adv. Electron. Mater. 5 (6) (2019) 1800904.
[8] D.A. Wright, Thermoelectric properties of bismuth telluride and its alloys, Nature 181 (4612) (1958) 834 (-834).
[9] A.F. Al Naim, F.L. Supian, A.G. El-Shamy, Bismuth telluride (Bi_2Te_3) nanoparticles as a brilliant microwave absorber: a new exploration, J. Alloy. Compd. 899 (2022) 163271.
[10] Y. Zhang, Q. You, W.C. Huang, L.P. Hu, J.F. Ju, Y.Q. Ge, H. Zhang, Few-layer hexagonal bismuth telluride (Bi_2Te_3) nanoplates with high-performance UV-Vis photodetection, Nanoscale Adv. 2 (3) (2020) 1333–1339.
[11] Y.C. Liu, J.D. Chen, C. Wang, H.Y. Deng, D.M. Zhu, G.J. Hu, X.S. Chen, N. Dai, Bulk photovoltaic effect at infrared wavelength in strained Bi_2Te_3 films, APL Mater. 4 (12) (2016) 126104.
[12] H.J. Zhang, C.X. Liu, X.L. Qi, X. Dai, Z. Fang, S.C. Zhang, Topological insulators in Bi_2Se_3, Bi_2Te_3 and Sb_2Te_3 with a single Dirac cone on the surface, Nat. Phys. 5 (6) (2009) 438–442.
[13] Y.L. Chen, J.G. Analytis, J.H. Chu, Z.K. Liu, S.K. Mo, X.L. Qi, H.J. Zhang, D.H. Lu, X. Dai, Z. Fang, S.C. Zhang, I.R. Fisher, Z. Hussain, Z.X. Shen, Experimental realization of a three-dimensional topological insulator, Bi_2Te_3, Science 325 (5937) (2009) 178–181.
[14] R. Subedi, G. Guisbiers, Synthesis of ultrawide band gap TeO2 nanoparticles by pulsed laser ablation in liquids: top ablation versus bottom ablation, ACS Omega (2024).
[15] G. Guisbiers, Selenium: a critical chemical element in nano and quantum physics, Adv. Phys. X 9 (2024) 2357809.
[16] S. Barcikowski, V. Amendola, G. Marzun, C. Rehbock, S. Reichenberger, D. Zhang, B. Gökce. Handbook of Laser Synthesis of Colloids, 2016.
[17] D.S. Zhang, B. Goekce, S. Barcikowski, Laser synthesis and processing of colloids: fundamentals and applications, Chem. Rev. 117 (5) (2017) 3990–4103.
[18] P. Srivastava, K. Singh, Low temperature reduction route to synthesise bismuth telluride (Bi2Te3) nanoparticles: structural and optical studies, J. Exp. Nanosci. 9 (10) (2014) 1064–1074.
[19] M.S. Rider, M. Sokolikova, S.M. Hanham, M. Navarro-Cia, P.D. Haynes, D.K.K. Lee, M. Daniele, M.C. Guidi, C. Mattevi, S. Lupi, V. Giannini, Experimental signature of a topological quantum dot, Nanoscale 12 (2020) 22817.
[20] R.P. Panmand, G. Kumar, S.M. Mahajan, N. Shroff, B.B. Kale, S.W. Gosavi, Growth of Bi_2Te_3 quantum dots/rods in glass: a unique highly stable nanosystem with novel functionality for high performance magneto optical devices, Phys. Chem. Chem. Phys. 14 (47) (2012) 16236–16242.
[21] E.E. Foos, R.M. Stroud, A.D. Berry, Synthesis and characterization of nanocrystalline bismuth telluride, Nano Lett. 1 (12) (2001) 693–695.
[22] J. Tyndall, The Glacier of the Alps, Longmans Green & Co., 1896.
[23] S. Bhattacharjee, DLS and zeta potential – what they are and what they are not? J. Control. Release 235 (2016) 337–351.
[24] I. Bejenari, V. Kantser, A.A. Balandin, Thermoelectric properties of electrically gated bismuth telluride nanowires, Phys. Rev. B 81 (7) (2010) 075316.
[25] L.D. Geoffrion, G. Guisbiers, Quantum confinement: size on the grill!, J. Phys. Chem. Solids 140 (2020).
[26] K.M.F. Shahil, M.Z. Hossain, D. Teweldebrhan, A.A. Balandin, Crystal symmetry breaking in few-quintuple Bi2Te3 films: applications in nanometrology of topological insulators, Appl. Phys. Lett. 96 (2010) 153103.
[27] L. Ren, X. Qi, Y.D. Liu, G.L. Hao, Z.Y. Huang, X.H. Zou, L.W. Yang, J. Li, J.X. Zhong, Large-scale production of ultrathin topological insulator bismuth telluride nanosheets by a hydrothermal intercalation and exfoliation route, J. Mater. Chem. 22 (11) (2012) 4921–4926.
[28] J. Yuan, M. Zhao, W.Z. Yu, Y. Lu, C.Y. Chen, M. Xu, S.J. Li, K.P. Loh, Q.L. Bao, Raman spectroscopy of two-dimensional $Bi_2Te_xSe_{3-x}$ platelets produced by solvothermal method, Materials 8 (8) (2015) 5007–5017.
[29] J.M. Raju, K.J. Thomas, Topological insulator phases in polycrystalline Bi_2Te_3 thin films, AIP Adv. 13 (2023) 025045.
[30] J. Tauc, Optical properties and electronic structure of amorphous Ge and Si, Mater. Res. Bull. 3 (1968) 37–46.
[31] J. Tauc, R. Grigorovici, A. Vancu, Optical properties and electronic structure of amorphous germanium, Phys. Status Solidi b 15 (1966) 627–637.
[32] G. Guisbiers, Advances in thermodynamic modelling of nanoparticles, Adv. Phys.-X 4 (1) (2019).